A STUDY OF NONLINEAR EDDY-VISCOSITY MODELS IN A FLOW SOLVER FOR TURBOMACHINERY [1]

B. Wickerath
Institute of Jet Propulsion and Turbomachinery
RWTH Aachen University
Templergraben 55, D-52062 Aachen
Email: wickerath@ist.rwth-aachen.de,

R. Niehuis
Institute of Jet Propulsion
University of Ferderal Armed Forces of Munich
Werner-Heisenberg-Weg 39, D-85577 Neubiberg
Email: reinhard.niehuis@unibw.de

Keywords: *turbomachinery; turbulence models; eddy-viscosity models; curvature; rotation*

Abstract

In the field of computational fluid dynamics for turbomachinery flow applications, two-equation eddy-viscosity models are widely used, as they integrate extensive physical aspects and require an acceptable amount of computer resources. In the area of turbomachinery they are used for flows in various blade configurations, whereas for each case slight advantages or disadvantages may be observed. Although computation results generally show good agreement with real flow quantities, serious deviations appear for complex geometries. Within the frame of the national cooperative project "Turbulente Strömungen mit starker Stromlinienkrümmung" (turbulent flows with strong streamline curvature) new approaches to turbulence modelling and model extensions were implemented in the Navier-Stokes Solver PANTA (RANS, URANS), which was developed at the Institute of Jet Propulsion and Turbomachinery at the RWTH Aachen University and tested on turbomachinery relevant cases. The objective was to derive improved turbulence models which lead to better flow simulations and predictions of flow quantities in the area of turbomachinery. Thereby, special consideration was given to the effects of streamline curvature. Various turbulence models and model extensions were investigated, which take into account the influence of rotation and streamline curvature. Here, a model extension for the parameterization of the eddy-viscosity coefficient - the method by Rung - and the Explicit Algebraic Reynolds Stress Model by Wallin and Johansson (EARSM) as well as an extension of the model proposed by Hellsten (EARSM-CC) are applied. The improvement potential and the deficits remaining further on of the examined models and model extensions are presented and evaluated.

1 General Introduction

In the frame of computational fluid dynamics for turbomachinery flow applications, solving the time-averaged conservation equations will probably be the method of choice over a long period of time even in the future. Although methods like

[1]The project forming the basis of this report was founded by the Federal Ministry of Education and Research (BMBF), Project No. 03NIA2AC1. The authors of this publication are responsible for its contents.

the Large Eddy Simulation (LES) and the Direct Numerical Simulation (DNS) of flows are starting to be applied, they are still limited to relatively low Reynolds numbers. Furthermore, they are computationally too expensive to be used on an every day basis in research and industry, although computational power is further growing. So, linear two-equation eddy-viscosity models are still dominant in the context of industrial flow computations.

Although viscous flow solvers have reached a high level of accuracy in simulating turbomachinery flows, deficits in the prediction of turbulent flow phenomena still exist. In flows with strong effects of streamline curvature, flow separation or system rotation, linear eddy-viscosity models may fail to give accurate predictions. However, such models are popular and their use in complex flows is widespread due to their formalistic simplicity, numerical robustness and computational economy.

The objective of the present work is to investigate nonlinear eddy-viscosity turbulence models in a flow solver for turbomachinery. This study focuses on the effects of streamline curvature and rotation in typical turbomachinery flows. For this purpose, the Boussinesq hypothesis of the linear eddy-viscosity models was extended by different approaches to sensitise the models to rotational and streamline curvature effects. In this context Rung[1] suggests to modify the eddy-viscosity coefficient c_μ by making it a function of velocity-gradient invariants. Furthermore, an Explicit Algebraic Reynolds Stress Model (EARSM) is applied to account for system rotation and streamline curvature. The EARSM replaces the Boussinesq eddy-viscosity assumption by a more general constructive relation for the second-order correlation in the Reynolds averaged Navier-Stokes equations. In this way, the linear Boussinesq hypothesis is extended by higher order terms.

These extensions of the linear eddy-viscosity models have been implemented into the three-dimensional, Reynolds averaged, compressible Navier-Stokes flow solver *PANTA*, which was developed at the Institute of Jet Propulsion and Turbomachinery of the RWTH Aachen University. All models have been validated using basic test cases such as a turbulent flat plate, a backward facing-step or a flow over an axially rotating cylinder.

The nonlinear eddy-viscosity models are applied to different test cases in the field of turbomachinery, such as a low pressure turbine cascade (not shown here), a transonic compressor cascade or an impeller of a centrifugal compressor stage. For this, calculations have been performed to evaluate the accuracy of prediction of the models mentioned above. The results of the calculations are compared with experimental data and the results obtained by using a conventional linear eddy-viscosity models. It is shown that the prediction of the simulations can be partially improved compared to the linear models, but deficits still exist in the prediction of boundary layers featuring transition phenomena.

2 Extension of current linear eddy-viscosity models

Existing linear eddy-viscosity models often cannot correctly predict the complex dynamics of inter-component transfer. In flows with strong streamline curvature, adverse pressure gradients, flow separation or system rotation, such models may fail to give accurate predictions. The main cause of this is the fact that the linear Boussinesq approach

$$\overline{\rho u_i' u_j'} = \frac{2}{3}\rho k \delta_{ij} - 2\rho c_\mu k \tilde{S}_{ij} \qquad (1)$$

relates the Reynolds stress tensor $\overline{\rho u_i' u_j'}$ linearly to the traceless strain rate tensor

$$\tilde{S}_{ij} = \frac{T_t}{2}\left(\frac{\partial u_i}{\partial x_j} + \frac{\partial u_j}{\partial x_i}\right) - \frac{T_t}{3}\frac{\partial u_k}{\partial x_k}\delta_{ij} \qquad (2)$$

and contains no explicit dependence on the rotation rate tensor

$$W_{ij} = \frac{T_t}{2}\left(\frac{\partial u_i}{\partial x_j} - \frac{\partial u_j}{\partial x_i}\right). \qquad (3)$$

Here, the strain rate and rotation rate tensor are normalized with the turbulent timescale T_t:

$$T_t = \begin{cases} \frac{k}{\varepsilon} & \text{k-}\varepsilon \text{ models} \\ \\ \frac{1}{\beta^*\omega} & \text{k-}\omega \text{ models } (\beta^* = 0.09) \end{cases} . \quad (4)$$

In the sense of the polynomial representation

$$\overline{\rho u_i' u_j'} = P(\delta_{ij}, \tilde{S}_{ij}, \tilde{S}_{ij}^2, \tilde{S}_{ik}W_{kj}, \tilde{S}_{jk}W_{ki}, W_{ij}^2, \ldots)$$

the Boussinesq hypothesis (1) takes only zeroth- and first-order terms of the velocity gradients into account. Thus, the equations expressed in a rotating coordinate system are identical to the ones written in a non-rotating system. Additionally, the effect of local rotation is lost, that could be related to the absence of rotation near stagnation points and the excessive rate of rotation within vortices. This is the major deficit of standard eddy-viscosity two-equation models and one of the reasons for the fact that such models fail in predicting the correct rate of turbulence production in complicated turbulent flows (Wallin[2]).

In order to sensitize eddy-viscosity models to rotational and streamline curvature effects, it is necessary to extend the linear Boussinesq assumption (1). Below, different models of varying complexities are presented. These models have been implemented into the three-dimensional compressible Navier-Stokes flow solver *PANTA*. Here, all models are used in conjunction with the Wilcox[6] low-Reynolds number k-ω model and have been validated with basic test cases.

2.1 Parameterization of the Eddy-Viscosity Coefficient c_μ

Basing on existing eddy-viscosity models, Rung[1] as well as Pettersson Reif[3] suggest to modify the eddy-viscosity coefficient c_μ in the computation of the turbulent viscosity $\mu_t = \rho c_\mu k T_t$ (see eq. (1)). While, conventionally, this c_μ coefficient has a constant value of 0.09, both methods express it as a function of the invariants of the mean strain and rotation rate tensor. By means of the realizability principle, Rung defines a functional relationship between the eddy-viscosity coefficient and the invariants. According to realizability restrictions, Rung[1] proposes the following formulation for the modified coefficient c_μ^{eff}:

$$c_\mu^{eff} = \frac{1}{A_0 + 3.84\Psi\sqrt{0.204S^2 + 0.796W^2}}, \quad (5)$$

where

$$\Psi = \cos\left(\frac{1}{3}\arccos\left[\frac{\sqrt{6}\eta_3}{\eta_1^{1.5}}\right]\right) \quad (6)$$

and

$$A_0 = 6.25\,(1 - \tanh[0.54S])\,. \quad (7)$$

Here η_1, η_3 and S represent invariants of the non-dimensional strain rate tensor $\tilde{S}_{ij}$ defined by (2):

$$\eta_1 = \tilde{S}_{ij}^2, \quad \eta_3 = \tilde{S}_{ij}^3, \quad S = \sqrt{2\eta_1} \quad (8)$$

and

$$W = \sqrt{2\tilde{W}_{ij}^2} \quad (9)$$

denotes the invariant of the modified rotation rate tensor $\tilde{W}_{ij}$ defined by:

$$\tilde{W}_{ij} = W_{ij} + 2T_t C_\omega \varepsilon_{jim}\Omega_m^{sys}. \quad (10)$$

The last term in the equation above (10) represents the influence of system rotation on the turbulent flow field. Ω_m^{sys} is the constant angular rotation rate vector of the coordinate system, $\varepsilon_{jim} = (j-i)(i-m)(m-j)/2$ denotes the cyclic permutation tensor and the constant C_ω is specified by Rung[1] to be 2.25.

As a result of relating the eddy-viscosity coefficient to the invariants of the strain rate and the rotation rate tensor, a non-linear dependence between the Reynolds stresses and the strain rate as well as rotation rate tensor is obtained. This method clearly enables the models based on the linear Boussinesq hypothesis (1) to account for rotational and streamline curvature effects. As aforementioned the method is used together with the low-Reynolds number k-ω model by Wilcox[6] and will be denoted by WI-RG in the following.

2.2 Explicit Algebraic Reynolds Stress Model (EARSM)

With the aid of Explicit Algebraic Reynolds Stress Models (EARSM), the linear Boussinesq hypothesis (1) may be replaced by a transport equation for the Reynolds stress anisotropy a_{ij}, which is defined as:

$$a_{ij} = \frac{\overline{\rho u_i' u_j'}}{\rho k} - \frac{2}{3}\delta_{ij} \tag{11}$$

An EARSM approach represents a systematic method of constructing a non-linear stress relationship that includes effects of the rotational part of the mean velocity gradient tensor. The Explicit Algebraic Reynolds Stress Model that is applied here is a variation of the EARSM described in detail by Wallin & Johansson[4].

Wallin and Johansson derive a linear transport equation for the Reynolds stress anisotropy from a recalibrated differential Reynolds stress model (Launder, Reece & Rodi[5] model). This relation is obtained by ignoring the advection and diffusion terms and employing a linear approach for the pressure-strain rate as well as by assuming an isentropic dissipation rate tensor. Finally, by using ten tensorially independent groups and five invariants, an implicit equation for the Reynolds stress anisotropy can be derived. For two-dimensional mean flows, this resulting equation is a cubic equation and can be solved in a closed form. As a solution an explicit expression for the Reynolds stress anisotropy tensor has been derived and represented as a function of the strain rate tensor $\tilde{S}_{ij}$ (see eq. (2)) and the rotation rate tensor $\tilde{W}_{ij}$ (see eq. (10)), as well as their invariants ($II_S, II_W, IV, \ldots$). From equation (11) the following expression for the Reynolds stress tensor is obtained:

$$\overline{\rho u_i' u_j'} = \frac{2}{3}\rho k\,\delta_{ij} - 2\rho c_\mu^{eff} k\,\tilde{S}_{ij} + \rho k a_{ij}^{(ex)}, \tag{12}$$

where the effective c_μ^{eff} coefficient is

$$c_\mu^{eff} = -\frac{1}{2} f_1 \left(\beta_1 + II_S \beta_6\right). \tag{13}$$

Thus, the Reynolds stresses are written in terms of the conventional Boussinesq approach (compare eq. (1)) and an extra anisotropy $a_{ij}^{(ex)}$:

$$\begin{aligned}
\underline{\underline{a}}^{(ex)} = {} & \left(1 - f_1^2\right) \frac{3B_2 - 4}{\max\left(II_S, II_S^{eq}\right)} \left(\underline{\underline{\tilde{S}}}^2 - \frac{1}{3} II_S \underline{\underline{\delta}}\right) \\
& + f_1^2 \beta_3 \left(\underline{\underline{\tilde{W}}}^2 - \frac{1}{3} II_W \underline{\underline{\delta}}\right) \\
& + \left(f_1^2 \beta_4 - \frac{\left(1 - f_1^2\right) B_2}{2\max\left(II_S, II_S^{eq}\right)}\right) \left(\underline{\underline{\tilde{S}}}\,\underline{\underline{\tilde{W}}} - \underline{\underline{\tilde{W}}}\,\underline{\underline{\tilde{S}}}\right) \\
& + f_1 \beta_6 \left(\underline{\underline{\tilde{S}}}\,\underline{\underline{\tilde{W}}}^2 + \underline{\underline{\tilde{W}}}^2\,\underline{\underline{\tilde{S}}} - II_S \underline{\underline{\tilde{S}}} - \frac{2}{3} IV \underline{\underline{\delta}}\right) \\
& + f_1^2 \beta_9 \left(\underline{\underline{\tilde{W}}}\,\underline{\underline{\tilde{S}}}\,\underline{\underline{\tilde{W}}}^2 - \underline{\underline{\tilde{W}}}^2\,\underline{\underline{\tilde{S}}}\,\underline{\underline{\tilde{W}}}\right).
\end{aligned} \tag{14}$$

By this formulation, relevant turbulent quantities are computed from a conventional two-equation eddy-viscosity model (here the low-Reynolds number k-ω model by Wilcox[6]). The contribution from the extra anisotropy is added as fully explicit additional terms in the equations. In order to sensitize the EARSM to rotational effects, similarly to the model by Rung, Wallin and Johansson proposed a modification of the rotation rate tensor $\tilde{W}_{ij}$ also represented in equation (10), whereas the EARSM model constant C_ω is set to 3.25.

The β coefficients that appear in equation (13) and (14) are functions of the invariants of the strain rate and the rotation rate tensor and are derived from the solution of the transport equation. The functional correlations as well as the constants used are to be found in the work of Wallin and Johansson[4]. It should be pointed out that the applied EARSM includes the extension for compressible mean flow effects as well as the near-wall correction described by Wallin and Johansson.

2.3 Streamline Curvature Correction of the Explicit Algebraic Reynolds Stress Model (EARSM-CC)

The literature contains examples on how to improve the described EARSM (see section 2.2) in order to properly simulate the rotational and streamline curvature effects in the

considered flow field. Rumsey, Gatski, and Morrison[7] prove that neglecting the advection of the Reynolds stress anisotropy is not entirely correct, especially for simulations with strong streamline curvature. The sensitivity to the streamline curvature is partially lost through the so-called weak-equilibrium assumption established in order to derive the Explicit Algebraic Reynolds Stress Model. It has been shown by several authors that, in principle, this deficiency can be partially overcome by assuming the weak-equilibrium in a suitable curvilinear, stream-following coordinate system. Several methods, more or less complex, can be used in order to determine such a suitable coordinate system. Here a strain-rate based method by Hellsten, Wallin, and Laine[8] is applied.

Based on a coordinate transformation the following modification of the rotation rate tensor W_{ij} (eq. (3)) in the EARSM takes place:

$$\tilde{W}_{ij} = W_{ij} + \frac{T_t}{A_0}\,\varepsilon_{ijm}\,\Omega_m^{(r)}. \qquad (15)$$

Technically, this relationship corresponds to the modification of the rotation rate tensor (eq. (10)) already described in section 2.2. However, here $\Omega_m^{(r)}$ does not represent the global angular rotation rate vector of the coordinate system, but the rotation rate vector of the local basis of the curvilinear coordinate system, in which the advection of the Reynolds stress anisotropy has a minimum and the weak-equilibrium assumption is best satisfied. The constant A_0 is specified by Hellsten, Wallin, and Laine[8] to be -0.72.

Assuming that the best approximation of neglecting the transport effects of the anisotropy tensor is obtained in a coordinate system, where also the transport effects of the strain rate tensor $\tilde{S}_{ij}$ have a minimum, the following expression for $\Omega_m^{(r)}$ is derived:

$$\Omega_m^{(r)} = A_{mj}^{-1}\tilde{S}_{pl}\dot{\tilde{S}}_{lq}\varepsilon_{pqj}, \qquad (16)$$

where A_{mj}^{-1} is

$$A_{mj}^{-1} = \frac{II_S^2\delta_{mj} + 12III_S\tilde{S}_{mj} + 6II_S\tilde{S}_{mi}\tilde{S}_{ij}}{2II_S^3 - 12III_S^2}. \qquad (17)$$

Here $\dot{\tilde{S}}_{lq} = D\tilde{S}_{lq}/Dt$ denotes the substantial derivative of the strain rate tensor $\tilde{S}_{lq}$. $II_S = \tilde{S}_{ij}\tilde{S}_{ji}$ and $III_S = \tilde{S}_{ij}\tilde{S}_{jk}\tilde{S}_{ki}$ are its second and third invariant.

3 Simulation Results

The models presented in this paper have been implemented into the flow solver *PANTA*, which was developed at the Institute of Jet Propulsion and Turbomachinery at the RWTH Aachen University (IST) and is well suited for the time-accurate simulation of flow phenomena in turbomachinery components (see, eg. Benetschik et al.[9] and Brouillet et al.[10]). *PANTA* is a 2D/3D structured multi-block, cell-centered, finite-volume-based code, which solves the Euler or Navier-Stokes equations for steady as well as unsteady flow problems. This solver is especially designed for sub- and transonic flows (approximate Riemann solver of Roe, MUSCL technique, TVD-limiter). The implicit time discretization of the differential equations permits large time steps and therefore a fast convergence of the solution. To allow for the simulation of turbulent and transitional flow phenomena, different two-equation turbulence models (low Reynolds number models) as well as algebraic transitions models have been implemented in the code.

The described turbulence models and extensions were validated by simulating geometrically simple flows such as over a turbulent flat plate, a backward-facing step or a turbulent boundary layer in an axially rotating cylinder. To conserve space, the results of these simulations will not be presented here. It should be pointed out that the accuracy of the implementation as well as the essential properties of the presented models were verified by these simple test cases.

In order to assess the performance of the improved models in the field of computational fluid dynamics for turbomachinery flow application, two of the test cases are considered in this section. Presented below are the simulation results of the three-dimensional flow in an annular compressor cascade (RGW) as well as the flow in a centrifugal impeller (RADIVER). The model by

Rung (WI-RG), the Explicit Algebraic Reynolds Stress Model by Wallin and Johansson (EARSM) and the curvature correction of the Explicit Algebraic Reynolds Stress Model (EARSM-CC) are used in conjunction with the k-ω model by Wilcox (WI). The results of the calculations are compared with existing experimental data and with simulation data obtained by use of the linear k-ω model.

Because of the well-known sensibility of the k-ω model to the free-stream values of ω, several calculations are performed with different boundary conditions for the turbulent length scale. Furthermore meshes with different resolutions were generated in order to assure that the solutions are grid-independent (not presented here).

3.1 Annular Compressor Cascade (RGW)

The experimental investigation of the first test case was carried out to examine the influence of blade loading on the three-dimensional flow in a subsonic annular compressor cascade. For this test case, the rotor has been removed from the test rig to assure an undisturbed, circumferentially uniform flow through the measuring cascade (Fig. 2). The compressor cascade consists of 24 untwisted blades with a hub-to-tip ratio of 0.75. Characteristic parameters of the cascade are summarized in Table 1. The experimental investigation was performed by Schulz and Gallus[11] at the Institute of Jet Propulsion and Turbomachinery at the RWTH Aachen University.

Number of blades	24
Tip diameter	428 *mm*
Hub diameter	321 *mm*
Stagger angle	29°
Chord	62.6 *mm*
Nominal deflection	29°
Aspect ratio	0.86
Pitch-to-chord ratio	0.78
Angle of attack at zero incidence	42°

Table 1 Cascade geometry data

Three-dimensional simulations were performed using an O-grid of 201x41x41 nodes, whereas the blade profile was described by 201 node points. The semi-viscous sublayer was solved with around 8 node points, so that the non-dimensional distance of the first cell has reached a value of $y^+ = 1..2$. Table 2 shows the boundary conditions that have been applied for all simulations.

Inlet:	
Total pressure	107000 *Pa*
Total temperature	309 *K*
Angle of attack	40°
Mach number	0.29
Turbulence intensity	1.3%
Turbulent length scale	0.2 *mm*
Outlet:	
Static pressure	102100 *Pa*

Table 2 Boundary conditions used for the simulation of the guide vane

Fig. 1 presents the non-dimensional pressure distribution developed on the blade surface at midspan. The predictions by the Explicit Algebraic Reynolds Stress Models (EARSM and EARSM-CC) as well as the extension by Rung (WI-RG) are compared with experimental data

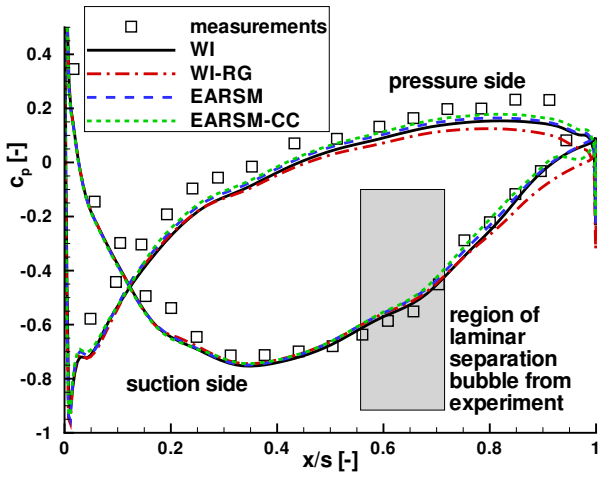

Fig. 1 Non-dimensional pressure coefficient at midspan

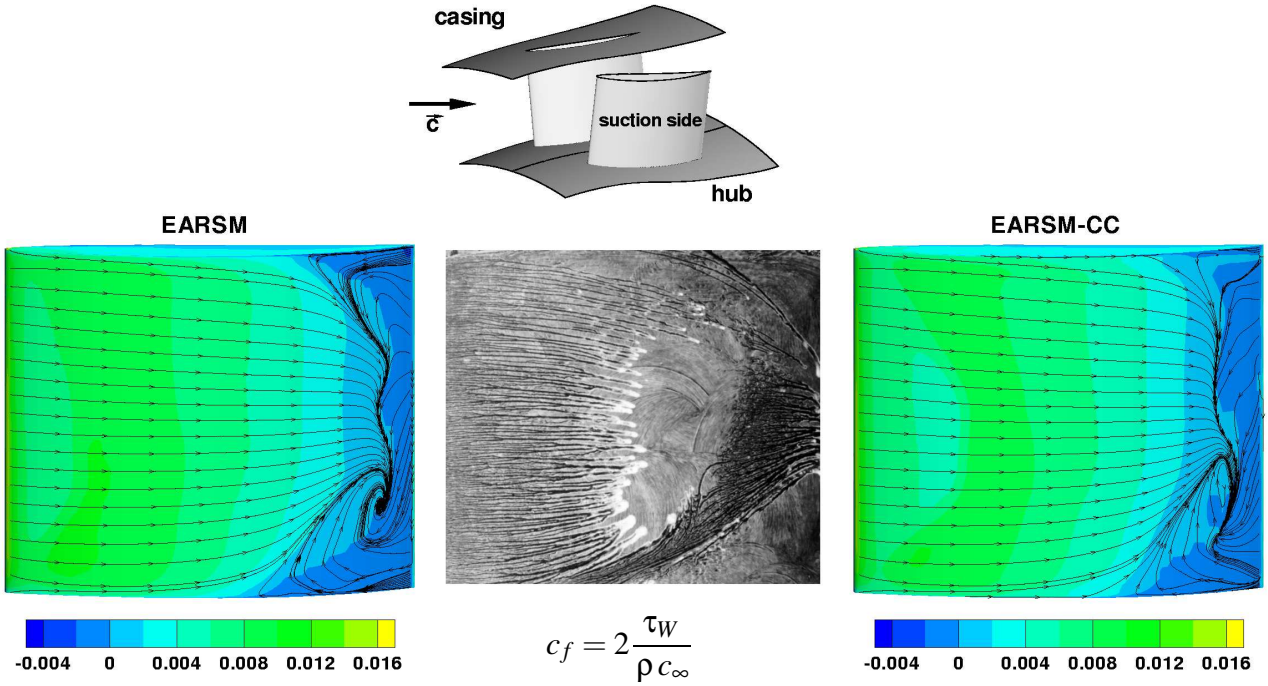

Fig. 2 Oil flow visualization and predicted skin-friction coefficient at the blade suction side

and the simulation made by the conventional linear Wilcox model (WI). It can clearly be seen that the calculated pressure distributions vary only slightly from each other except at the trailing edge. Here, especially the model by Rung (WI-RG) shows major differences in the pressure distribution compared to the Wilcox model. Moreover, all of the models predict the pressure side distribution very well and match the experimental results quite well, whereas the curvature correction of the Explicit Algebraic Reynolds Stress Model (EARSM-CC) gives the best agreement with the experimental data. The pressure distribution on the suction side of the blade is also well simulated by all models. Both Explicit Algebraic Reynolds Stress Models predict the pressure distribution almost identically. Compared to the results obtained by the linear Wilcox model (WI), the EARSMs show a slight improvement in the back region of the profile, unlike the model proposed by Rung (WI-RG).

The experimental data in Fig. 1 indicates that on the suction side the flow continuously accelerates from the leading edge until about 35 percent of the chord length ($x/s = 0.35$). Here, the boundary layer is laminar until about 55 percent of the chord where the laminar boundary layer separates and reattaches as a turbulent boundary layer. The pressure plateau of the suction side

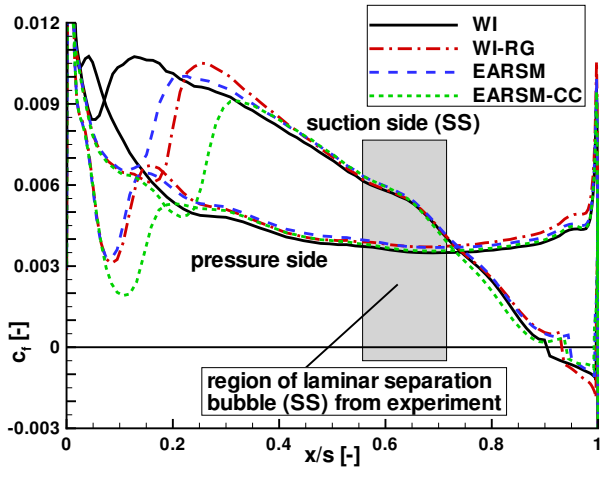

Fig. 3 Skin-friction coefficient at midspan

(Fig. 1) indicates the formation of this separation bubble and the flow visualization shown in Fig. 2 confirms this conclusion.

Considering Fig. 2 and Fig. 3, it is obvi-

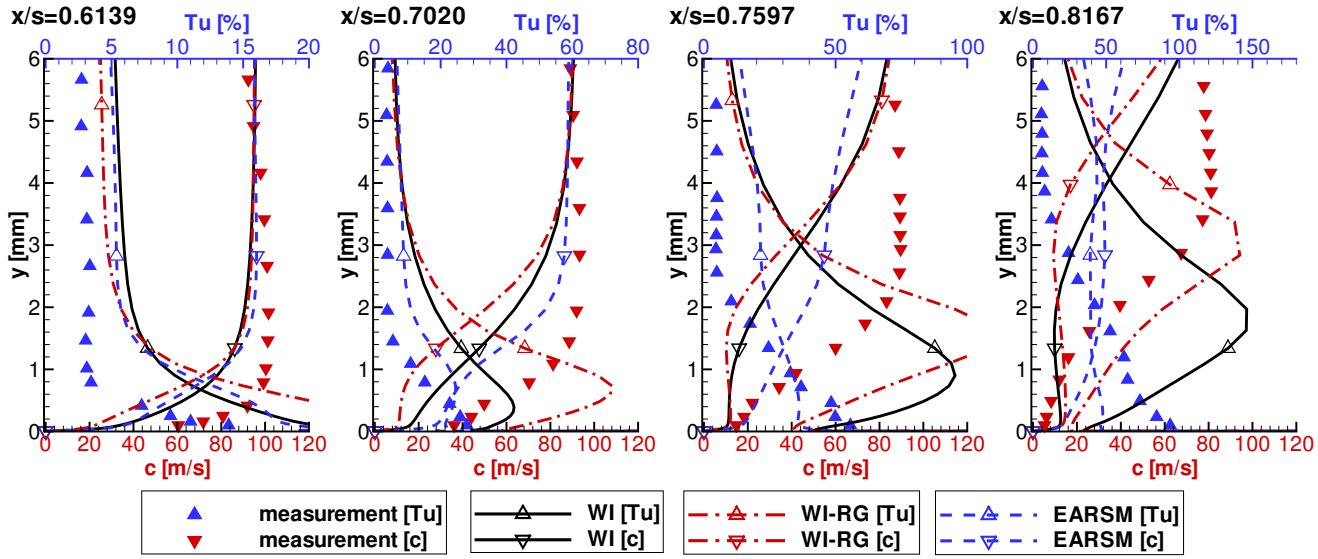

Fig. 4 Turbulence intensity and velocity profiles of the blade suction side boundary layer (13% span)

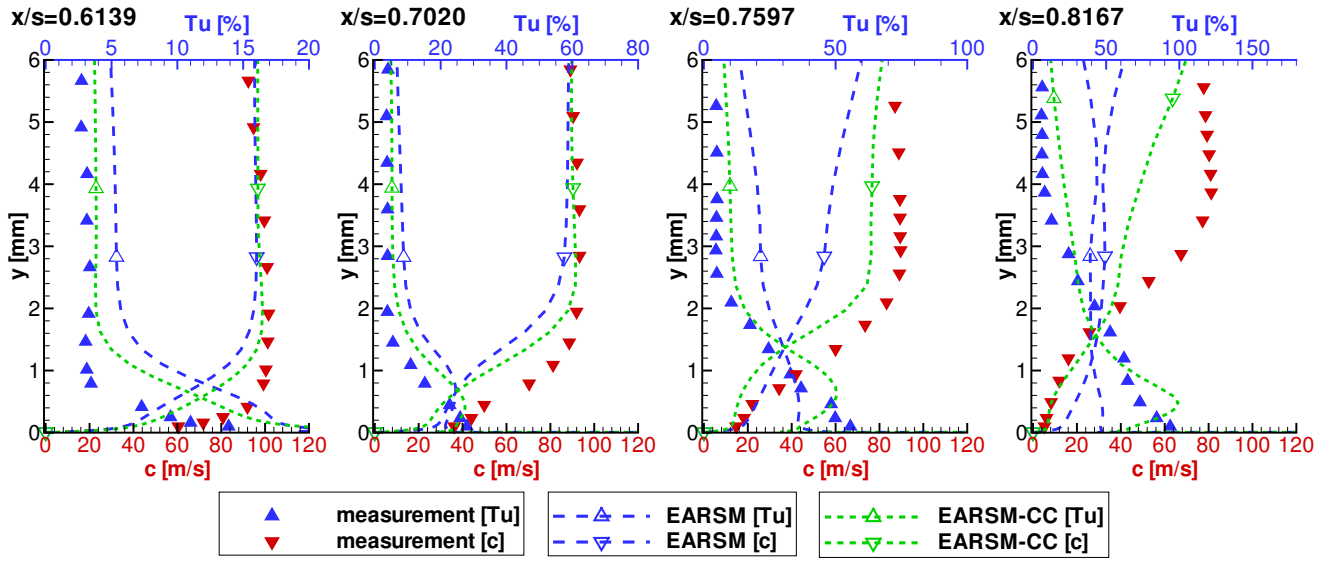

Fig. 5 Turbulence intensity and velocity profiles of the blade suction side boundary layer (13% span)

ous that all investigated turbulence models fail to predict this separation bubble. From Fig. 3 it can be seen that for all models the calculated skin-friction coefficient c_f, at midspan, decreases from its maximum at the leading edge towards a local minimum, where the boundary layer undergoes transition and the skin-friction coefficient increases again. Next c_f decreases due to the deceleration of the flow and falls to zero once the flow approaches a turbulent separation at the trailing edge. However, the numerical simulations predict the transition from laminar to turbulent flow too early. Regardless of the model used, this transition occurs in the front area of the blade profile, closer to leading edge. In Fig. 3 it can be seen that the model proposed by Rung (WI-RG) and the Explicit Algebraic Reynolds Stress Model (EARSM) predict the occurrence of the

laminar-turbulent flow transition later than the conventional Wilcox model (WI). The curvature correction following Hellsten (EARSM-CC) provides further improvement, predicting this transition even further downstream. However, when compared to experimental data (Fig. 2), this model predicts the transition too early as well. The premature transition to turbulence prevents the flow separation, because a turbulent boundary layer has less tendency to separate than a laminar one. Therefore, the non-linear turbulence models also fail to reliably simulate the real flow phenomena. The simulation results obtained by Thermann et al.[12] and Thermann and Niehuis[13] confirm that this deficiency arises due to the transition to turbulence. With the aid of transition models using the intermittency concept, Thermann was able to simulate the separation bubble on the suction side correctly. Nevertheless, also in his simulations, contrary to the experimental data, the trailing edge separation also appeared.

The surface flow visualization in Fig. 2 suggests significant secondary flows, partially being responsible for the hub corner separation on the suction side. The cross passage flow at the hub moves upstream, close to the suction surface, and generates a vortex with a clockwise orientation. The endwall corner separations on the suction side, the one at the hub and the smaller one at the casing, are the primary three-dimensional features of this test case. Although the Explicit Algebraic Reynolds Stress Models still have deficiencies in the laminar-turbulent flow transition, they are characterized by significant improvements in the prediction of strong secondary flows. Especially in the boundary layer near the hub (see Fig. 4), the EARSM performs considerably better than the linear k-ω model (WI) and the model proposed by Rung (WI-RG). Compared to the basic model (EARSM), also in this case, the curvature correction (EARSM-CC) provides results which remain in better agreement with the experimental data (Fig. 5). However, in spite of these improvements, no significant influence on the pressure distribution is noticed.

3.2 Impeller of a centrifugal compressor

In the following, the transonic flow through the impeller of a centrifugal compressor operating under real application conditions is considered (Fig. 6). This test case is characterized by a high

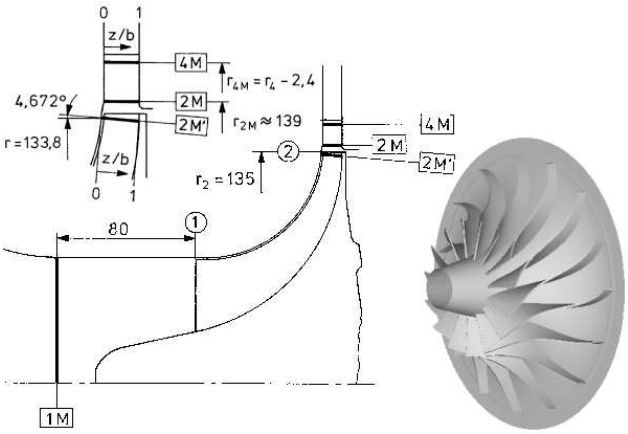

Fig. 6 Impeller and measuring planes (Ziegler[16])

number of revolutions, a large boundary layer as well as a large influence of secondary flows and Coriolis effects. Therefore the flow configuration poses a severe challenge to turbulence modeling.

Number of blades	15
Tip diameter	270 *mm*
Meridional diffuser height	11 *mm*
Blade backsweep angle	38°
Rotational speed at design point	35640 $\frac{1}{min}$
Maximum total pressure ratio	4.07
Maximum mass flow	1.46 $\frac{kg}{s}$
Isentropic efficiency of impeller	90.8 %

Table 3 Technical data of compressor

The compressor is part of a test rig that has been designed at the Institute of Jet Propulsion and Turbomachinery at the RWTH Aachen University to study interaction phenomena of impeller and diffuser by Ziegler et al.[14]-[16]. Therefore, most of the measurements were carried out with a vaned diffuser. Nevertheless, the base of the current computations is the experimental data, which has been conducted with a

vaneless diffuser. The compressor consists of an unshrouded impeller with 15 backswept blades developed by MTU Aero Engines. Some technical data is summarized in Table 3. A detailed description of the compressor and the test rig is given by Ziegler[16].

Inlet:	
Total pressure	$60000\,Pa$
Total temperature	$295\,K$
Number of revolutions	$28510\,\frac{1}{min}$
Mach number	0.7
Turbulence intensity	2.0%
Turbulent length scale	$0.2\,mm$
Outlet:	
Static pressure	$\approx 135000\,Pa$

Table 4 Boundary conditions used for the simulation of the impeller

The compressor is run in a closed loop. Thus, it is possible to vary the inlet pressure and temperature. In the present case the absolute total inlet pressure is about $0.6\,bar$ and the number of revolutions is 80% of the rotational speed at design point. Further boundary conditions of the considered operating point are shown in Table 4.

The computational mesh consists of four blocks. Assuming rotational symmetry only one blade channel is meshed using an O-type tip clearance grid and also an O-type grid around the blade. Inflow and outflow of the impeller are meshed with H-type grids. The grid is refined both at the blade surface and at hub and casing, such that the averaged distance of the first cell y^+ has a value of about 1.5. The calculations were performed with a mesh that consists of 48 cells from hub to casing (14 in the area of the clearance gap). The O-grid in the blade channel inside the impeller has 300 cells around the blade and 26 cells perpendicular to the blade surface. The entire mesh consists of about 475.000 cells.

Fig. 7 presents the measured total pressure ratio Π_t and the total isentropic efficiency η_t of the impeller for different mass flows at 80% speed (Table 4). As well, the results of various turbulence models are shown for the operating point P1 (see Fig. 7) which was experimentally investigated in much detail.. Varying the static pressure at the outlet, the mass flow of the calculations were adjusted to the measurements. Obviously all models predict the total pressure ratio higher than in the experiment (Fig. 7). Whereas the isentropic efficiency is underestimated by the Explicit Algebraic Reynolds Stress Models (EARSM and EARSM-CC) and overestimated by the other models (WI and WI-RG). It can be

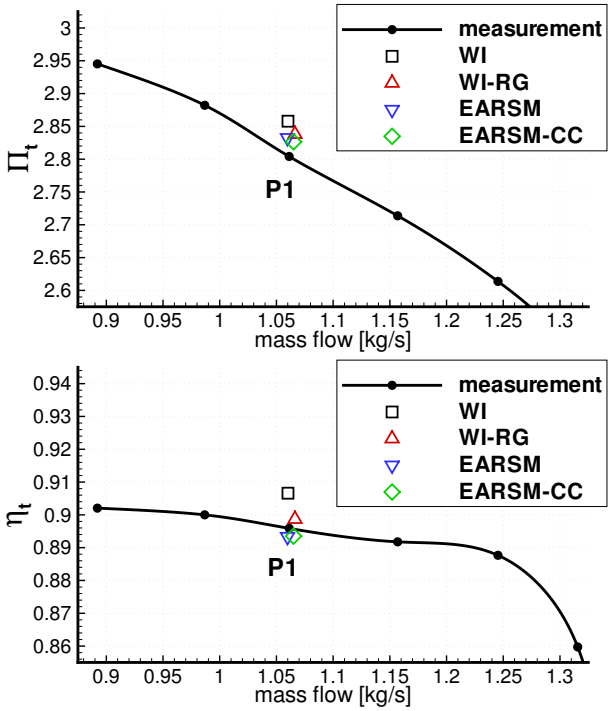

Fig. 7 Impeller characteristic: Total pressure ratio Π_t and total isentropic efficiency η_t

seen that the predictions obtained from the model by Rung (WI-RG) and the Explicit Algebraic Reynolds Stress Model (EARSM) are closer to the measurements than those obtained by the conventional Wilcox model (WI). As in the previous test case, also here the curvature correction (EARSM-CC) provides results which are in better agreement with the experimental data compared to the basic model (EARSM). Nevertheless, all examined models show a good agreement with the experiment which indicates that the important physical phenomena inside the impeller are well represented by all numerical simulations.

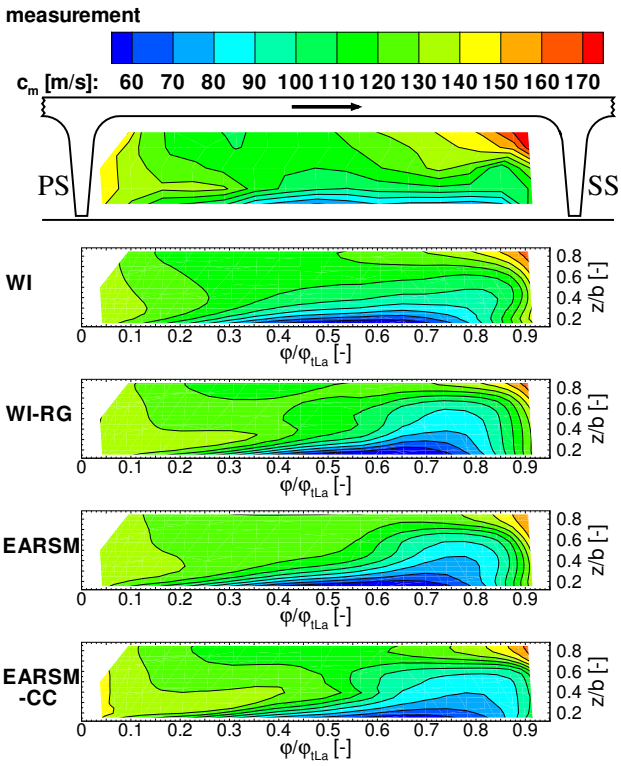

Fig. 8 Meridional velocity c_m at plane 2M'

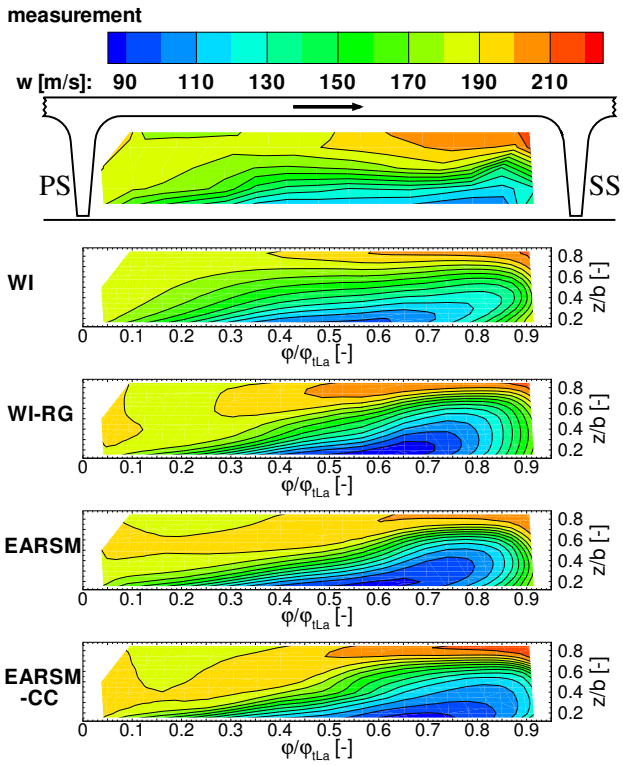

Fig. 9 Relative velocity w at plane 2M'

In order to confirm this conclusion the analysis of the flow field in the measuring plane 2M' which is close to the exit of the impeller (see Fig. 6) is carried out at the considered operating point P1. Therefore the calculated flow properties of the different turbulence models are compared in plane 2M' with Laser-2-Focus measurements. At first, in Fig. 8 the meridional velocity is displayed. The flow field is characterized by an area of low meridional velocity that is located at the front wall. Applying the linear k-ω model (WI), this area is slightly larger in the simulation than in the experiment, but the overall prediction of the meridional velocity is very good. However, the extension of the area of low meridional velocity is overpredicted by the model proposed by Rung (WI-RG) as well as by both Explicit Algebraic Reynolds Stress Models (EARSM and EARSM-CC). With increasing complexity of the models the circumferential center of this area moves from the center of the flow channel closer to the suction side.

Considering the relative velocity (Fig. 9), one can see that again the overall predictions of all examined models are good. However, the calculated extensions of the wake region which is represented by the area of low relative velocity are also too large. As in the case of the meridional velocity, the wake region is shifted more and more towards the suction side using higher-order models. With respect to the wake region, the Wilcox model gives the best agreement with the measured axial extension of the region whereas the curvature corrected Explicit Algebraic Reynolds Stress Model (EARSM-CC) provides the best prediction of the location. A possible reason for the calculated large extension of the wake region is, that the clearance flow is too large in the simulation (see also Weiß et al.[17]). This can be attributed either to a deficient flow simulation or to a different clearance height, which has only been measured for the non-rotating impeller.

As can be seen from Fig. 10, the non-linear models (WI-RG, EARSM and EARSM-CC) provide significant improvements in the prediction

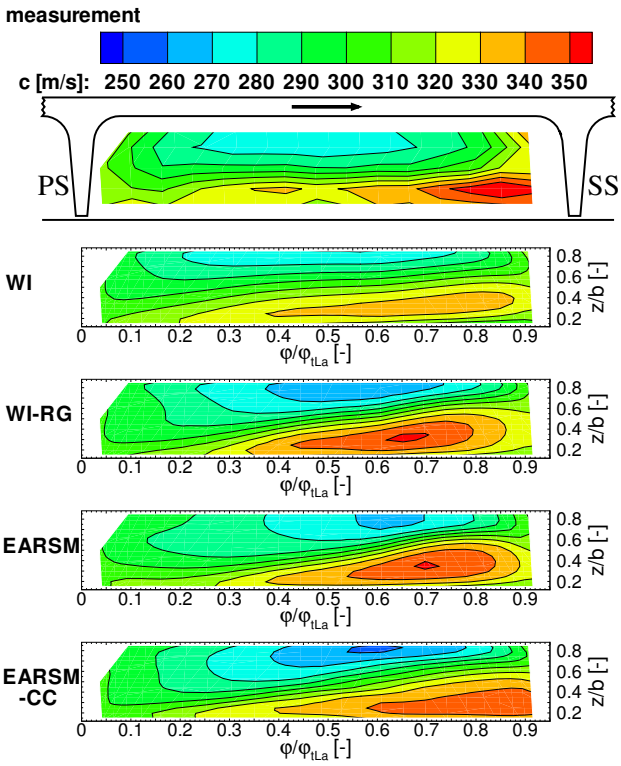

Fig. 10 Absolute velocity c at plane 2M'

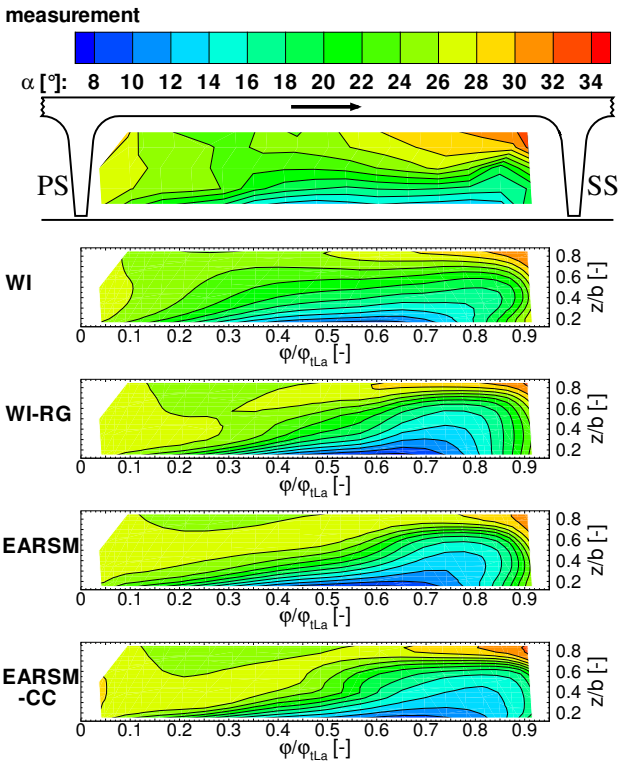

Fig. 12 Absolute flow angle α at plane 2M'

of the absolute velocity. Especially the small region of high absolute velocity that is located in the corner of the suction side and front wall, is in better agreement with the experimental data compared to the linear k-ω model (WI). The area of low absolute velocity which is located at the rear wall is predicted slightly too large in the pressure region and too small nearby the suction side.

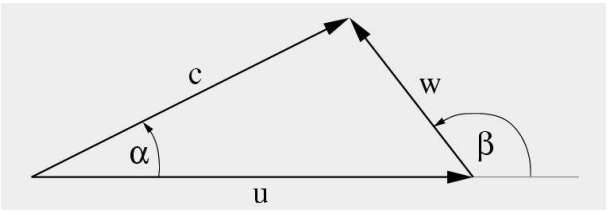

Fig. 11 Flat velocity triangle

The differences in the accuracy of the predicted velocities become more obvious when regarding the flat velocity triangle described in Fig. 11. Variations of the absolute flow angle α (especially at constant absolute velocity c and at small values of α) cause significant changes in meridional velocity c_m and relative velocity w but only small changes in relative flow angle β and circumferential velocity c_u. Considering Fig. 12 and Fig. 13, it is obvious that especially in the wake region the non-linear models improve the prediction of the relative flow angle β while these models give less accurate results for the absolute flow angle α than the linear k-ω model. Moreover, the Explicit Algebraic Reynolds Stress Models (EARSM and EARSM-CC) and the model proposed by Rung (WI-RG) improve the prediction of the absolute velocities while they worsen the prediction of the relative velocities. Nevertheless, also with regard to improvements in the prediction of global parameters, the higher-order models show slight advantages in the current test case.

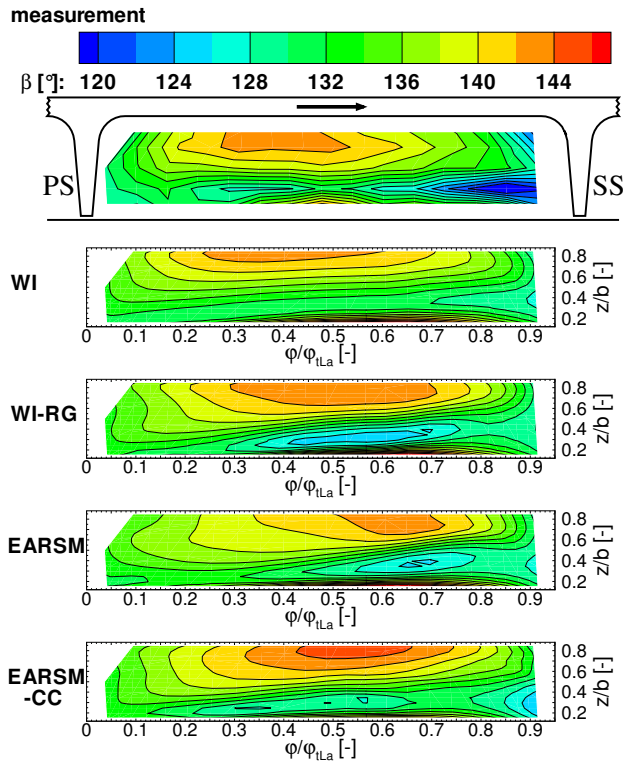

Fig. 13 Relative flow angle β at plane 2M'

4 Summary

The purpose of this work was to analyze the improvements offered by new models and model extensions in terms of eddy viscosity modeling in computational fluid dynamics for turbomachinery flow applications. At the moment, modeling of rotational and streamline curvature effects poses a challenge to existing turbomachinery flow solvers. The influence of these phenomena on the flow cannot be disregarded and, hence, the attempts for their incorporation into currently existing turbulence modeling schemes.

The previous simulations confirms the applicability of the low Reynolds number linear Wilcox model as a viable way to predict turbulence in various turbomachinery flows. Therefore, this model proves as an excellent basis in order to develop more robust two-equation model extensions able to take rotational and streamline curvature effects into account.

Thus, the described models, the parameterization of the eddy-viscosity coefficient by Rung (WI-RG), the Explicit Algebraic Reynolds Stress Model by Wallin and Johansson (EARSM) as well as its extension proposed by Hellsten (EARSM-CC) are all based on the linear Boussinesq approach, also used for the Wilcox model (WI).

The current simulations with the use of newly developed schemes provides interesting findings. In terms of simulating the rotational and streamline curvature effects on the flow field, these models offer certain improvements when compared to conventional linear eddy viscosity models. However, their use in computational fluid dynamics has only a slight influence on improving the prediction of global flow parameters such as the pressure ratio and the efficiency. Especially in flow simulations through cascades, where the blades are highly loaded, the applied models fail to reliably predict the laminar-turbulent flow transition.

However, these models show a significant improvement when compared to a conventional linear eddy viscosity model. The Explicit Algebraic Reynolds Stress Model by Wallin and Johansson (EARSM) promises certain improvements in simulating strong secondary flow field. Here additional improvements are clearly seen by using the curvature corrected Explicit Algebraic Reynolds Stress Model (EARSM-CC).

Nomenclature

a_{ij}	Reynolds stress anisotropy tensor
$a_{ij}^{(ex)}$	extra Reynolds stress anisotropy tensor
c	absolute velocity
c_m	meridional velocity
c_f	skin-friction coefficient
c_μ	eddy-viscosity coefficient
c_μ^{eff}	modified eddy-viscosity coefficient
f_1	damping function
k	turbulent kinetic energy
$\overline{\rho u_i' u_j'}$	Reynolds stress tensor
$\tilde{S}_{ij}$	non-dimensional strain rate tensor
T_t	turbulent time scale
Tu	turbulence intensity

u_i	velocity in cartesian coordinates
u	circumferential velocity
w	relative velocity
W_{ij}	rotation rate tensor
x_i	cartesian coordinates
x/s	dimensionless chord length
y	wall distance
y^+	dimensionless wall distance
z/b	dimensionless channel height
$II_S = \tilde{\mathbf{S}}^{\mathbf{2}}$	invariant of the non-dimensional strain rate tensor
$III_S = \tilde{\mathbf{S}}^{\mathbf{3}}$	invariant of the non-dimensional strain rate tensor
$IV = \tilde{\mathbf{S}}\tilde{\mathbf{W}}^{\mathbf{2}}$	invariant of the non-dimensional strain rate and rotation tensor

greek:

α	absolute flow angle
β	relative flow angle
β_i	model coefficients
δ_{ij}	Kronecker-Delta
η_t	total isentropic efficiency
$\eta_1 = \tilde{S}_{ij}^2$	invariant of the non-dimensional strain rate tensor
$\eta_3 = \tilde{S}_{ij}^3$	invariant of the non-dimensional strain rate tensor
ε	turbulent dissipation rate
ε_{ijk}	cyclic permutation tensor
μ_t	turbulent viscosity
$\Omega_m^{(r)}$	rotation rate vector of the local basis of the curvilinear coordinate system
Ω_m^{sys}	constant angular rotation rate vector of the coordinate system
Π_t	total pressure ratio
ρ	density
$\overline{\rho u_i' u_j'}$	Reynolds stress tensor

References

[1] Rung, T.: *Realizability linearer stress-strain Beziehungen, Institutsbericht Nr. 04/98*, Hermann-Fötteringer-Institut für Strömungsmechanik, TU Berlin, 1998.

[2] Wallin, S.: *Engineering turbulence modelling for CFD with a focus on explicit algebraic Reynolds stress models. Dissertation*, KTH Stockholm, 2000.

[3] Pettersson Reif, B.A.; Durbin, P.A.; Ooi A.: *Modeling rotational effects in eddy-viscosity closures*, International Journal of Heat and Fluid Flows 20 (1999), pp. 563-573, 1999.

[4] Wallin, S.; Johansson, A.V.:: *An explicit algebraic Reynolds stress model for incompressible and compressible turbulent flows*, J. Fluid Mech. 403, pp. 89-132, 2000.

[5] Launder, B.E.; Reece, G.J.; Rodi W.: *Progress in the development of a Reynolds stress turbulence closure*, Journal of Fluid Mechanics, Vol. 68, 1975.

[6] Wilcox, D.C.: *Simulation transition with a two-equation turbulence model*, AIAA J. 32, pp.247-255, 1994.

[7] Rumsey, C. R.; Gatski, T. L.; Morrison, J. H.: *Turbulence model predictions of extra-strain rate effects in strongly-curved flows*, AIAA Paper (1999), pp. 99-157, 1999.

[8] Hellsten, A.; Wallin, S.; Laine, S.: *Scrutinizing curvature corrections for algebraic Reynolds stress models*, AIAA-paper 2002-2963, 32nd AIAA Fluids Dynamics Conference, St. Louis, Missouri, 2002.

[9] Benetschik, H.; Lohmann, A.; Lücke, J.R.; Gallus H.E.: *Inviscid and viscous analysis of three-dimensional turbomachinery flows using an implicit upwind algorithm*, AIAA 96-2556. 1996.

[10] Brouillet, B.; Benetschik, H.; Volmar T.; Gallus, H.E.; Niehuis, R.: *3D Navier-Stokes simulation of a transonic flutter cascade near stall conditions*, in Tamaru T. (ed.),Procceeding of the Int. Gas Turbine Congress Kobe, Japan, no. 1, pp. 511-518, 1999.

[11] Schulz, H.D.; Gallus, H.E.: *Experimental investigation of the influence of rotor wakes on the development of the profile boundary layer and the performance of an annular compressor cascade*, AGARD 74th (A) Specialist Meeting on Unsteady Aerodynamic Phenomena in Turbomachines, 1989.

[12] Thermann, H.; Müller, M.; Niehuis, R.; Skoda, R.; Schilling, R.: *Numerical simulation of the flow in an annular compressor cascade with different turbulence and transition models*, 5th European Conference on Turbomachinery Fluid Dynamics and Thermodynamics, Prague, Czech Republic, 2003.

[13] Thermann, H.; Niehuis, R.: *Unsteady Navier-Stokes simulation of a transonic flutter cascade near stall conditions applying algebraic transition models*, ASME GT2005-68221, Proceedings of ASME Turbo Expo 2005, Nevada, USA, 2005.

[14] Ziegler, K.U.; Gallus, H.E.; Niehuis, R.: *A Study on Impeller-Diffuser Interaction: Part I - Influence on the Performance*, ASME Paper GT-2002-30381, 2002.

[15] Ziegler, K.U.; Gallus, H.E.; Niehuis, R.: *A Study on Impeller-Diffuser Interaction: Part II - Detailed Flow Analysis*, ASME Paper GT-2002-30382, 2002.

[16] Ziegler, K. U. : *Experimentelle Untersuchung der Laufrad-Diffusor-Interaktion in einem Radialverdichter variabler Geometrie*, Dissertation RWTH Aachen, 2003.

[17] Weiß , C.; Grates, D.R.; Thermann, H.; Niehuis, R.: *Numerical investigation of the influence of the tip clearance on wake formation inside a radial impeller*, ASME GT2003-38279, Proceedings of ASME Turbo Expo 2003, Atlanta, USA, 2003.